Green Synthesis Method and Application of NaP Zeolite Prepared by Coal Gasification Coarse Slag from Ningdong, China

Wenxin Ji [1,2,*], Shiyue Zhang [1], Pengde Zhao [1], Shasha Zhang [2], Ning Feng [1], Liping Lan [2], Xiaoguang Zhang [2,*], Yonggang Sun [1,2], Yuanyuan Li [1,2] and Yulong Ma [1,2]

[1] State Key Laboratory of High-efficiency Utilization of Coal and Green Chemical Engineering, Ningxia University, Yinchuan 750021, China
[2] College of Chemistry and Chemical Engineering, Ningxia University, Yinchuan 750021, China
[*] Correspondence: jwx@nxu.edu.cn (W.J.); ndzhangxg@126.com (X.Z.); Tel.: +86-135-1957-9989 (W.J.); +86-139-9521-8798 (X.Z.)

check for updates

Abstract: In view of the current and urgent environmental protection needs, the use of industrial solid waste in China's Ningdong is becoming more and more important. In this paper, NaP zeolite with good physical properties is synthesized by using coal gasification coarse slag (CGCS) as the raw material, without the addition of a silicon and aluminum source, without the addition of a template agent, and without high-temperature calcination. Add a small amount of NaOH and deionized water to the CGCS to adjust the molar ratio to $SiO_2:Al_2O_3:Na_2O:H_2O = 5.2:1.0:5.0:100$. The effects of aging time, crystallization temperature, and crystallization time parameters on synthetic zeolite were studied. The raw materials and the obtained zeolite were tested by XRF, XRD, SEM, FT-IR, TG-DSC, BET, and other technologies. The results show that the specific surface area of the synthesized NaP zeolite can reach 161.06 m^2/g, which has the characteristics of large specific surface area, regular morphology, and high crystallinity. We obtained NaP zeolite through a simple and low-cost synthesis method. The synthesized NaP zeolite was used to simulate the removal of ammonia nitrogen in wastewater, and the optimal removal rate was 92.67%. Among them, Na^+ plays an important role in the synthesis of NaP zeolite and ion exchange with NH_4^+. Our research provides new ideas for solving the large-scale accumulation of CGCS and treating ammonia nitrogen in industrial wastewater. Thus, it is a promising green environmental protection and "treating waste by waste" route.

Keywords: coal gasification coarse slag; NaP zeolite; ammonia nitrogen; green environmental

1. Introduction

With the huge impact of global climate change on the human living environment, the clean and efficient use of coal is particularly important. At present, China's clean coal mainly uses coal gasification and other technologies. Coal gasification slag (CGS) is the solid waste generated by the entrained-flow coal gasification technology. According to different pathways of formation, it consists of two forms (coarse slag and fine slag). Coal gasification technology has been widely used for the demand for energy, but the problem of solid waste and water pollution is becoming more and more serious [1,2]. Ningdong energy and chemical base is one of the most advanced bases for developing clean coal technology in China. In 2018, the base generated nearly 8 million tons of CGS [3]. At present, there is no good treatment method, and it can only be landfilled after high-standard anti-seepage treatment on the ground, which is quite different from the systematic utilization of fly ash [4–8]. This treatment not only occupies land resources, causes enormous environmental pressure, but also brings

high transportation and processing costs to the enterprise. Therefore, it is especially important to realize the "zero emission" [9] of coal gasification technology and to find ways to recycle CGS.

At present, there are many researches on the resource utilization of fly ash and slag in the world [7,8,10]. However, since the CGS is obtained in a high-pressure vaporization furnace under a reducing atmosphere (CO, H_2) and 1400–1500 °C, its structure and composition are greatly different from those of fly ash and slag [3,5,9]. Therefore, it is difficult to realize the utilization of CGS by the same method. In this new field, only a few researchers have studied the application of CGS in porous materials, but they have not paid much attention to its resource utilization [11–14]. Although they have also synthesized excellent porous materials, their preparation process is still considered to have shortcomings such as high production cost, complicated process, easy secondary pollution and high energy consumption. At present, there are many methods for treating wastewater using solid waste, but they cannot be applied on a large scale due to the "cost and system integration" problem. Therefore, it is especially important to study a resource-based gasifier slag technology with low cost, simple process, low energy consumption, minimal secondary pollution and high system integration, and this technology will have high application value in the future.

This study is based on China Ningdong coal gasification coarse slag (CGCS) [3,15,16]. We hope to find a feasible way for the utilization of CGCS with the increasingly severe environmental pressure. NaP zeolite is synthesized by a low-cost green template-free method (the best process is shown in Figure 1): CGCS is used as the raw material, no additional silicon-aluminum source is required, and no high-temperature calcination is required. Add a small amount of sodium hydroxide and deionized water and mix well, then age and crystallize. The effects of different molar ratios, aging time, crystallization temperature and other parameters on the synthesis of zeolite were investigated. The crystal type, morphology, specific surface area, and pore structure of the product were analyzed and tested by a characterization method, whereby it was found that the specific surface area of the synthesized NaP zeolite was up to 161.06 m^2/g. The prepared NaP zeolite was used to remove ammonia nitrogen from simulated wastewater. The effect of pH, adsorption time, and adsorbent dosage on the removal efficiency was briefly studied, and the optimum removal rate was 92.67%. This research can realize the in-situ treatment and utilization of waste generated by the factory, avoid the transportation cost, and realize "treating waste by waste", which provides a new way for the recycling of CGCS and the treatment of ammonia nitrogen in industrial wastewater.
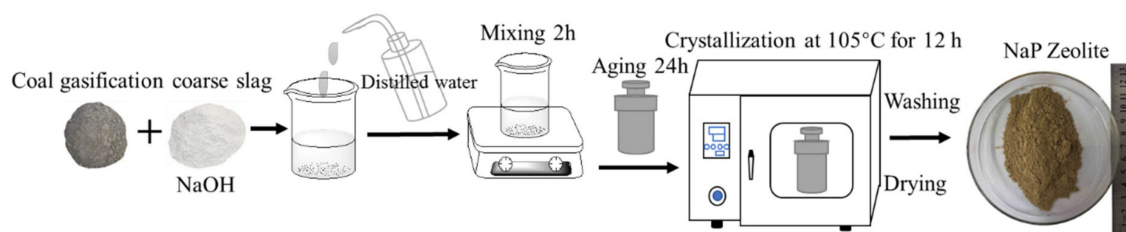

Figure 1. Schematic diagram of preparation process of NaP zeolite.

2. Experimental

2.1. CGCS and Reagent

The CGCS used in this study came from Ningdong Energy and Chemical Industry Base (Yinchuan, China). Chemical reagents: sodium hydroxide, non-hydrated sodium metasilicate, aluminum powder, hydrochloric acid, sodium potassium tartrate, anhydrous ammonium chloride are of analytical grade (purity > 99.5%), purchased from Shanghai (Sinopharm Chemical Reagent Co., Ltd, Shanghai, China). Among them, anhydrous sodium metasilicate and aluminum powder were only used to study the effect of SiO_2/Na_2O and SiO_2/Al_2O_3 on the performance of synthetic zeolite. Hydrochloric acid, sodium potassium tartrate, and anhydrous ammonium chloride were used for the ammonia nitrogen adsorption experiment. Prepared before the use of Nessler's reagent, purchased from Shanghai

(Maclean Biochemical Technology Co., Ltd, Shanghai, China). Dissolve anhydrous ammonium chloride in deionized water to obtain simulated ammonia nitrogen wastewater.

2.2. Synthesis of NaP Zeolite

Amorphous silica and alumina in CGCS are used as the silicon source aluminum source, and zeolite is synthesized without adding any template and without high temperature calcination. Grinding and sieving the raw material select a part with a particle size of less than 75 μm. Add 0.33 g NaOH and 3 mL deionized water to 1 g CGCS to adjust $SiO_2:Al_2O_3:Na_2O:H_2O = 5.2:1.0:5.0:100$. The mixture was then transferred to a 100 mL stainless steel autoclave (polytetrafluoroethylene lined) and aged for 6–72 h at room temperature. The autoclave was sealed and placed in an oven at 80–130 °C for 6–72 h. Rinse with distilled water until neutral, dry at 105 °C for 6 h, and store under seal.

2.3. Sample Characterization

X-ray fluorescence spectroscopy (XRF) studied the chemical composition of CGCS by using a S2 Ranger type (Bruker, Karlsruhe, Baden-Wurttemberg, Germany) spectrometer. The crystal phase of the solid product was subjected to X-ray diffraction (XRD) studies using a D8 advance type diffractometer (Bruker, Karlsruhe, Baden-Wurttemberg, Germany). The CuKα radiation source operates at voltages of 40 kV and 40 mA. The 2θ range was 5–50° and the scan rate is 2°/min. The scanning electron microscopy (SEM) was carried out by using JSM-7500F (JEOL, Tokyo, Japan) to study the morphology and structure of the composite materials. Fourier transform infrared spectroscopy (FT-IR) analysis in a Spectrum Two type (PerkinElmer, Waltham, MA, USA) spectrometer using KBr tablets. Thermogravimetric (TG)/differential scanning calorimetry (DSC) analysis was performed using a STA 449 F5 (Netzsch, Nuremberg, Bavaria, Germany) synchronous thermal analyzer with a heating rate of 10 °C/min. The N_2 adsorption-desorption isotherm curve was obtained at −196 °C using an ASAP2020 physical adsorption analyzer (Micromeritics, Norcross, GA, USA). The specific surface area was determined by BET equation, and the pore size distribution was calculated by N_2-DFT model. Prior to this analysis, the samples were evacuated at 200 °C for 2 h.

2.4. Ammonia Nitrogen Removal Experiment

The NaP zeolite washed to neutrality (aged for 24 h and crystallized at 105 °C for 12 h) was selected for ammonia nitrogen adsorption. The zeolite was added to a simulated ammonia nitrogen solution having a volume of 100 mL and a concentration of 100 mg/L (temperature: 25 °C, oscillation frequency: 180 r/min). The effects of adsorbent dosage, solution pH and adsorption time on ammonia nitrogen removal rate and adsorption capacity were studied. The mixture was centrifuged and filtered under different conditions. The ammonia nitrogen concentration in water was determined by Nessler's reagent method according to the Chinese National Standard (HJ 535-2009) [17], and the ultraviolet-visible spectrophotometer (UV-1800, Shimadzu, Tokyo, Japan) was at a wavelength of 420 nm. The formula for ammonia nitrogen removal rate and adsorption is as follows:

$$T(\%) = \frac{C_0 - C_e}{C_0} \times 100\% \tag{1}$$

$$Q(mg/g) = \frac{C_0 - C_e}{M} \times V \tag{2}$$

where T is the removal rate, Q is the adsorption amount, C_0 (mg/L) is the initial ammonia nitrogen concentration, C_e (mg/L) is the equilibrium ammonia nitrogen concentration, M (g) is the amount of adsorbent added, and V (L) is the volume of ammonia nitrogen wastewater.

2.4.1. Influence of Adsorbent Dosage

Adding 0.5–40 g/L NaP zeolite to the solution, adjusting the pH of the solution to 7 and the adsorption time of 180 min, the effect of adsorbent dosage on the ammonia nitrogen removal rate was studied. The removal rate and adsorption amount are calculated by using Equations (1) and (2).

2.4.2. Influence of pH

In order to study the effect of pH on ammonia nitrogen removal rate, 1 M NaOH and 1 M HCl were added to adjust the solution pH to 3–10. The previously determined 20 g/L NaP zeolite was added and the adsorption time was 180 min. Equation (1) was used to calculate the ammonia nitrogen removal rate at different pH values.

2.4.3. Influence of Adsorption Time

Twelve time points were selected within 5–480 min to study the effect of adsorption time on ammonia nitrogen removal rate. The previously determined 20 g/L NaP zeolite was added to adjust the solution pH to 7. Equation (1) is used to calculate the removal rate of ammonia nitrogen at different adsorption times.

3. Results and Discussion

3.1. XRF Result Analyses

The chemical composition of the CGCS sample is shown in Table 1. It can be found that the main components in CGCS are metal oxides, non-metal oxides and unburned carbon. Among them, SiO_2 + Al_2O_3 + Fe_2O_3 + CaO > 92%. By calculation, the molar ratio of SiO_2/Al_2O_3 in the CGCS can be obtained as 5.2.

Table 1. Chemical composition of coal gasification crude slag (CGCS) by XRF analysis (wt%) LOI is loss on ignition.

Parameter	SiO_2	Al_2O_3	Fe_2O_3	CaO	K_2O	MgO	Na_2O	Other	LOI
CGCS	53.44	17.21	11.23	10.12	2.27	1.92	1.33	2.48	12.55

3.2. XRD Result Analysis

3.2.1. Influence of SiO_2/Na_2O Molar Ratio

Figure 2a is an XRD spectrum with an initial gel composition of $5.2SiO_2{:}1.0Al_2O_3{:}xNa_2O{:}100H_2O$, in which the molar ratio of SiO_2/Na_2O is controlled to be 1.00–1.50 by adjusting the amount of NaOH added. When the molar ratio of SiO_2/Na_2O is increased from 1.00 to 1.04, the product changes from an amorphous phase to a characteristic peak of NaP zeolite. As the molar ratio further increases to 1.13, the crystallinity of the NaP zeolite gradually increases. Appropriate OH^- groups can promote the dissolution of amorphous gel, shorten the induction period, and accelerate the growth of NaP zeolite crystals [18,19]. When the SiO_2/Na_2O molar ratio reaches 1.50, the characteristic peak of the NaP zeolite is still significant, but the crystallinity is slightly decreased, which is related to the large negative charge density in the skeleton structure [20].
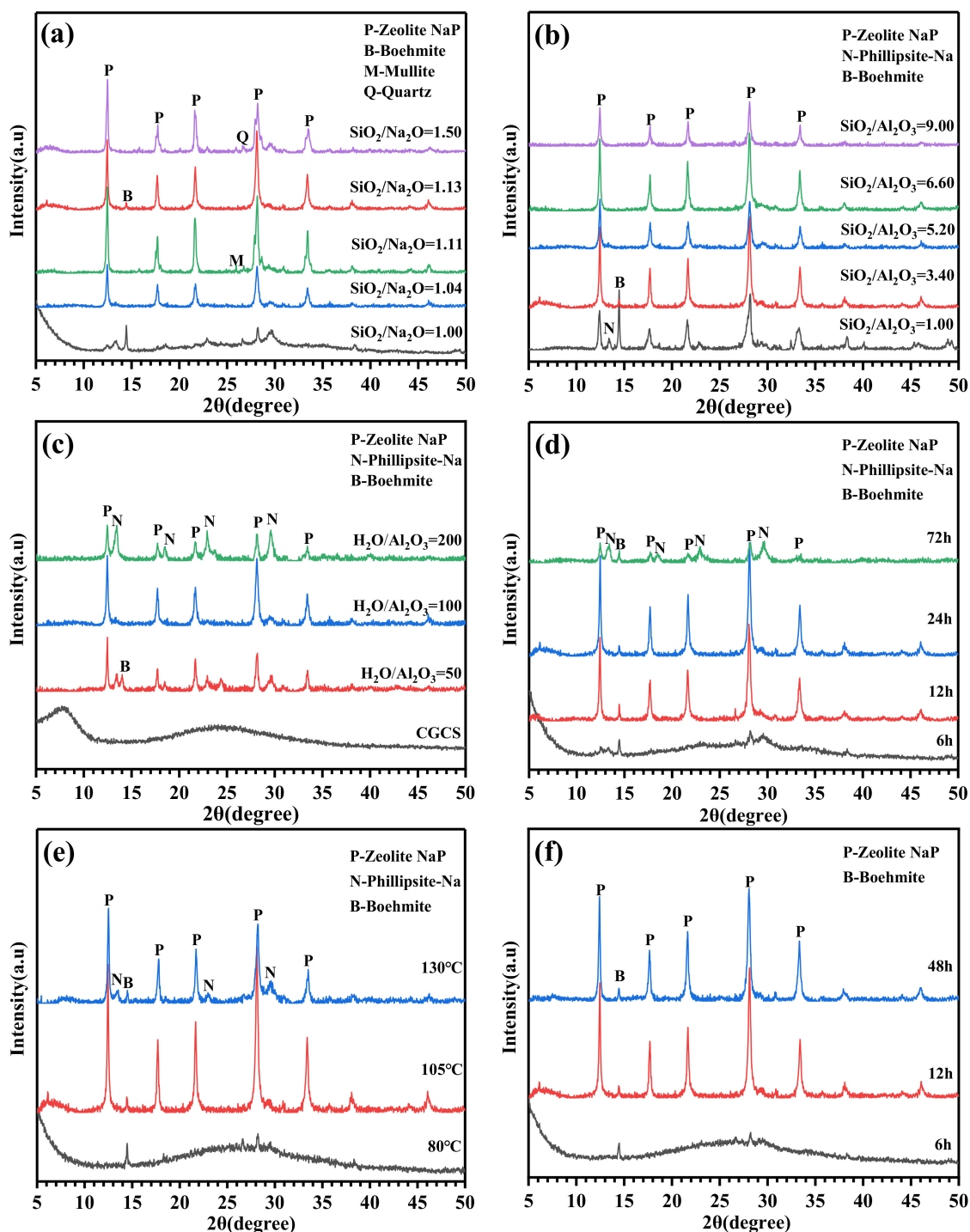
Figure 2. XRD patterns of CGCS and NaP zeolite synthesized under different conditions: (**a**) different SiO_2/Na_2O molar ratio, (**b**) SiO_2/Al_2O_3 molar ratio, (**c**) H_2O/Al_2O_3 molar ratio, (**d**) aging time, (**e**) crystallization temperature, (**f**) crystallization time.

3.2.2. Influence of SiO_2/Al_2O_3 Molar Ratio

Figure 2b shows the XRD spectrum of the synthesized product at a molar ratio of SiO_2/Al_2O_3 = 1.00–9.00 Although we use the method without adding exogenous silica-alumina to prepare zeolite, the silica-alumina ratio is still an important factor in zeolite synthesis. Therefore, we still investigated the change of the final product under different silicon-aluminum ratios by adding exogenous silicon-aluminum. The initial gel composition is $xSiO_2:1.0Al_2O_3:5.0Na_2O:100H_2O$. When

the molar ratio of SiO_2/Al_2O_3 = 1.00, the crystallinity of the NaP zeolite is insufficient, and the characteristic peak of the boehmite is very prominent, accompanied by a peak of Phillipsite-Na zeolite. As the molar ratio of SiO_2/Al_2O_3 increases, the boehmite gradually weakens. Until the molar ratio was 5.20, the boehmite disappeared completely and the product tended to be converted only to NaP zeolite. At this time, we did not adjust the silica-alumina molar ratio of CGCS. Since the relative solubility of Al^{3+} in alkaline NaOH solution is lower than that of Si^{4+}, the addition of a small amount of NaOH in a higher SiO_2/Al_2O_3 molar ratio promotes the formation of NaP zeolite [21]. When the molar ratio reached 9.00, the crystallinity of the NaP zeolite began to decrease because the amount of NaOH was too small to accelerate the reaction.

3.2.3. Influence of H_2O/Al_2O_3 Molar Ratio

Figure 2c is an XRD pattern of the synthesized products of CGCS and different H_2O/Al_2O_3 molar ratios. The initial gel composition is $5.2SiO_2:1.0Al_2O_3:5.0Na_2O:xH_2O$, where the range of x was adjusted by adding deionized water to 50–200. It can be seen from the XRD spectrum that there is no obvious crystalline phase in CGCS, and the materials such as silicon aluminum are mainly in the amorphous form, which further proves that the inorganic minerals are almost completely melted during the coal gasification process. When the molar ratio of H_2O/Al_2O_3 is 50, NaP zeolite, Phillipsite-Na and sodalite can be observed in the sample, and the characteristic peak of NaP zeolite is prominent. When the ratio is increased to 100, the NaP zeolite becomes the main crystalline phase. When the H_2O/Al_2O_3 molar ratio was further increased to 200, two crystal forms of Phillipsite-Na and NaP zeolite appeared in the sample. Therefore, we believe that the optimum H_2O/Al_2O_3 molar ratio of synthetic NaP zeolite is 100.

3.2.4. Influence of Aging Time

Figure 2d shows the XRD patterns of the synthesized products at different aging times (6–72 h). It can be seen from the XRD spectrum that when the aging time is 6 h, CGCS basically does not react. With the aging time increasing to 12–24 h, NaP zeolite becomes the main crystalline phase and contains only a small amount of boehmite. When the time is further increased to 72 h, NaP zeolite will decompose and Phillipsite-Na appears. If the time is too long, it will cause amorphization or crystal transition due to its own pressure. Therefore, aging for 24 h can shorten the induction period and reach the maximum crystallinity.

3.2.5. Influence of Crystallization Temperature

Figure 2e shows the XRD patterns of the synthesized products at different hydrothermal crystallization temperatures (80–130 °C). It can be seen that the crystallinity below 80 °C is insufficient and no crystalline phase appears. Because the temperature is too low, CGCS does not react with NaOH, and it is difficult to form a new crystal phase. When the temperature is raised to 105 °C and 130 °C, the characteristic peak intensity of the NaP zeolite first reaches the maximum and then decreases overall, and the strength decrease is caused by the decrease of the grain size [21]. Therefore, the crystallinity of NaP zeolite obtained at 105 °C is the highest.

3.2.6. Influence of Crystallization Time

Figure 2f shows the XRD patterns of the synthesized products at different hydrothermal crystallization times (6–48 h) at 24 h and 105 °C. It can be seen that when the crystallization time is 6 h, CGCS does not react and remains amorphous. When the crystallization time is 12–48 h, NaP zeolite becomes the main crystalline phase, because of long-term pressure of the amorphous phase, the crystallinity of zeolite decreases with time [21]. Therefore, the optimal crystallization time to reach the maximum crystallinity is 12 h.

The above conclusions confirm that, after the CGCS and NaOH solution are thoroughly mixed, activated molecules of SiO_2 and Al_2O_3 will be formed on the surface, and the interaction between the two will cause the active ingredients in CGCS to fall off the particle surface. When the alkaline solution

is heated, the active components of the unit cell grid are destroyed by OH^-. The Si-O-Al and Si-O-Si bonds on the surface of the particles break, and new $Si(OH)_5^-$ equipotential ions are formed, causing the surface of the particles to be negatively charged. Under the action of static electricity, Na^+ adheres to the solid particles in the solution. In addition, the active SiO_2 and Al_2O_3 react with Na^+ to form a hydrated sodium aluminosilicate gel and cover the surface of the CGCS, hinder the penetration and diffusion of active components, and reduce the diffusion speed of active molecules through the coating. The silicon–aluminum ratio leads to the continuous generation of crystal nuclei in the gel layer, and a complex and ordered grid-like channel structure appears, which is conducive to the diffusion of the molecules in the inner layer and accelerates the silicate condensation and crystallization. With the extension of time, crystal particles such as Na^+ accumulated on the surface of CGCS finally formed a stable NaP zeolite structure [22,23].

Based on the above results, we selected two NaP zeolites synthesized by adjusting the silicon-aluminum ratio ($SiO_2/Al_2O_3 = 3.40$) and experimental methods ($SiO_2/Al_2O_3 = 5.20$), and compared their performance differences under the same experimental conditions.

3.3. SEM Results Analysis

The morphology and particle size of the raw material CGCS and the prepared NaP zeolite were investigated by using different magnification SEM (Figure 3). The SEM micrograph of the original CGCS after thorough ground and mixed is irregularly granular and has no pore structure on the surface (Figure 3a). The NaP zeolite prepared by the green synthesis method has the characteristic structure of a rectangular prism crystal plane, which is consistent with the crystal morphology reported in the literature (Figure 3b,d) [24,25]. The morphology and average particle size of the samples were slightly different at different SiO_2/Al_2O_3 molar ratios. At a lower magnification, a honeycomb crystal polymer can be observed (Figure 3c). When the magnification is increased, about 4–7 μm "cauliflower-like" aggregates (Figure 3d) can be observed. These aggregates are composed of anisotropic growth of rectangular prismatic crystals with an average diameter of less than 1 μm [26].
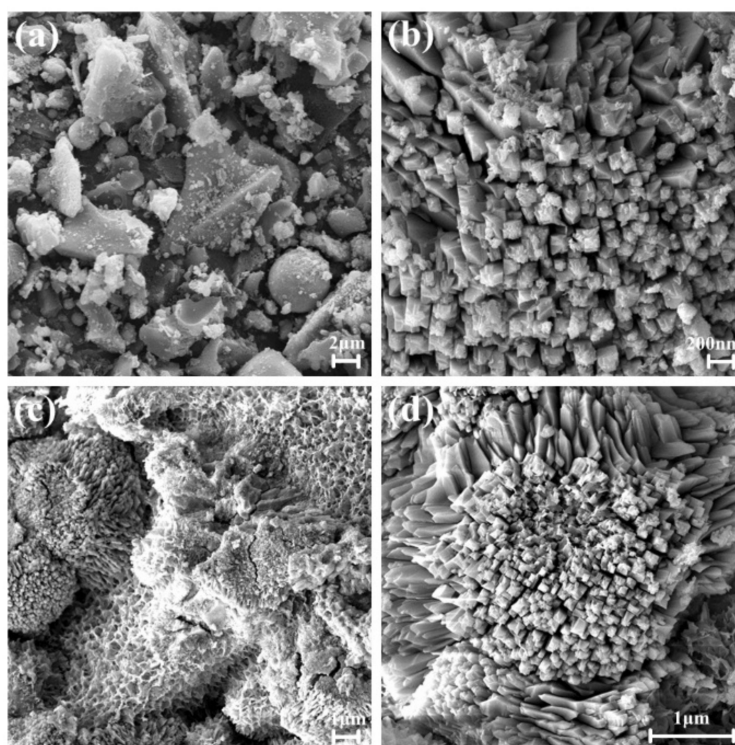

Figure 3. SEM images of CGCS and different SiO_2/Al_2O_3 molar ratio NaP zeolites: (**a**) CGCS, (**b**) $SiO_2/Al_2O_3 = 3.40$, (**c,d**) $SiO_2/Al_2O_3 = 5.20$.

3.4. FT-IR Result Analysis

Figure 4 is an FT-IR spectrum of a CGCS having a SiO_2/Al_2O_3 molar ratio of 5.20 and 3.40. The total vibration of the infrared spectrum of both samples is typical of NaP zeolite [27]. For the CGCS, the typical band near 1616 and 3444 cm^{-1} is assigned to the vibration of the hydroxyl groups of absorbed water [28]. In the spectrum of the SiO_2/Al_2O_3 molar ratios of 5.20 and 3.40, the bands around 1644 and 3448 cm^{-1} are caused by the solid phase hydrate in the hydroxyl group or the zeolite channel [22,29]. In the raw material CGCS and NaP zeolite, the bands around 1040 and 994 cm^{-1} are different. The former is a typical band of silicate glasses, which belongs to Si(Al)-O-Si anti-symmetric stretching, and the latter is caused by the asymmetric tensile vibration of YO_4 (Y = Si or Al) tetrahedron [30]. The former shifts to the latter of the lower wavenumber due to the alternating polycondensation of Si-O and Al-O bonds, or may be due to the reaction of the glass component in the CGCS with NaOH to form a zeolite structure [22,31]. The bands at 728 and 462 cm^{-1} in the raw material CGCS is a typical mullite vibrations [23]. The bands of 740, 673 and 438 cm^{-1} in the NaP zeolite are caused by the vibration of the internal tetrahedron or YO_4. The double ring present in the NaP zeolite backbone can be demonstrated by a band of 603 cm^{-1} [32]. The vibrational peaks of the infrared spectra of the two samples matched well with the typical NaP zeolite in the literature, confirming the successful synthesis of NaP zeolite [33,34].
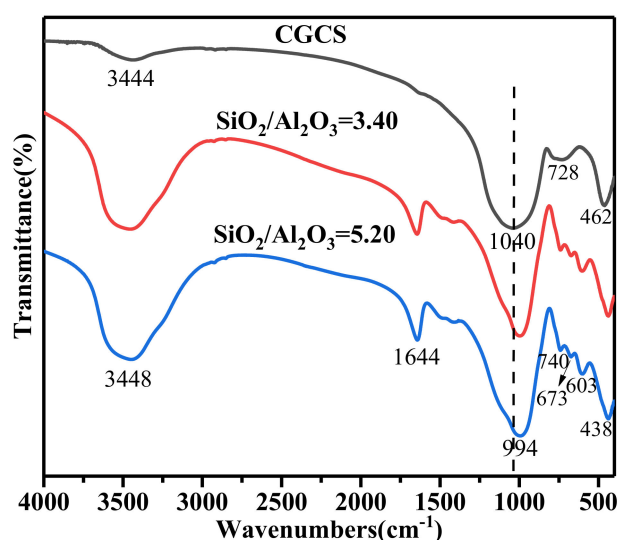

Figure 4. FT-IR spectra of CGCS and NaP zeolites with different SiO_2/Al_2O_3 molar ratios.

3.5. TG-DSC Results Analysis

Figure 5a,b shows the TG and DSC curves for NaP zeolite with different SiO_2/Al_2O_3 molar ratio. From the TG curve, the total weight loss was 13.20% and 15.44%, respectively, which is basically consistent with the shape and mass loss of the TG curve of the NaP zeolite reported in the literature [35]. In the temperature range of 20–200 °C, the removal of adsorbed water is the cause of mass loss. The removal and decomposition of hydroxyl groups in NaP zeolite will result in a mass loss between 200 and 500 °C [34]. Two thermal effects can be clearly seen from the DSC curve of the sample, and the endothermic peaks present at around 89 °C and 152 °C are related to the release of water molecules in the NaP zeolite. The exothermic effects at 386 °C and 364 °C are independent of weight loss and are due to the conversion and decomposition of the NaP zeolite structure [21,34,35]. Therefore, the heat resistant temperatures of our synthesized NaP zeolites were 386 °C and 364 °C.
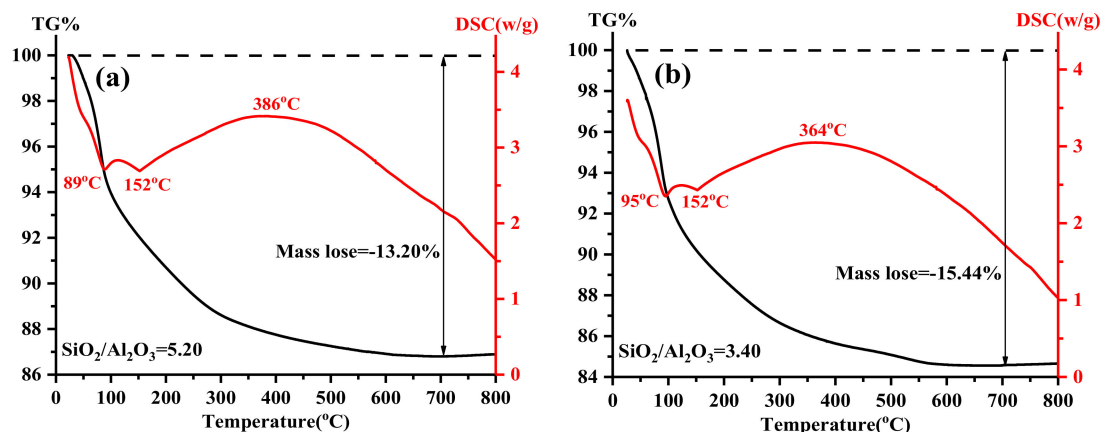
Figure 5. TG and DSC curves of different SiO_2/Al_2O_3 molar ratio NaP zeolites (**a**) 5.20, (**b**) 3.40.

3.6. BET Result Analysis

Table 2 shows the results of specific surface area, external surface area, total pore volume and average pore diameter of CGCS and different NaP zeolites after pretreatment at 200 °C. The specific surface areas of the SiO_2/Al_2O_3 = 5.20 and 3.40 samples were 161.06 m^2/g and 98.24 m^2/g, respectively, and the pore volumes were 0.0021 cm^3/g and 0.0036 cm^3/g, respectively. The sample with a molar ratio of 5.20 has a large specific surface area and a low pore volume, which is confirmed by XRD and SEM because of the small particle size of the sample [21,32].

Table 2. Structural parameters of NaP zeolite with CGCS and different SiO_2/Al_2O_3 molar ratios.

Sample	Surface Area (m^2/g)	External Surface Area (m^2/g)	Total Pore Volume (cm^3/g)	Average Aperture (nm)
CGCS	0.88	0.87	0.0013	18.05
SiO_2/Al_2O_3 = 3.40	98.24	88.99	0.0036	8.35
SiO_2/Al_2O_3 = 5.20	161.06	153.35	0.0021	5.57

The isotherm of the aperture type and distribution is shown in Figure 6. The pore size distribution of the NaP zeolite samples synthesized at different molar ratios was calculated using the N_2-DFT model. All samples exhibited a type IV isotherm with a H3 hysteresis loop (relative pressure range 0.45–0.99), which is a typical feature of mesoporous materials, where the hysteresis loop is related to the occurrence of pore condensation [36–38]. As can be seen from the dV/dW curve, samples were present as micropores and mesopores. According to SEM morphology analysis, the zeolite mesopores are caused by intercrystalline voids and intracrystalline mesopores in the crystal. There is a certain difference between the calculated area of the external surface area and the specific surface area, which further proves that the micropores and the mesopores coexist in the obtained zeolite [39]. The experimental results show that it has good consistency with typical NaP zeolite [40,41].
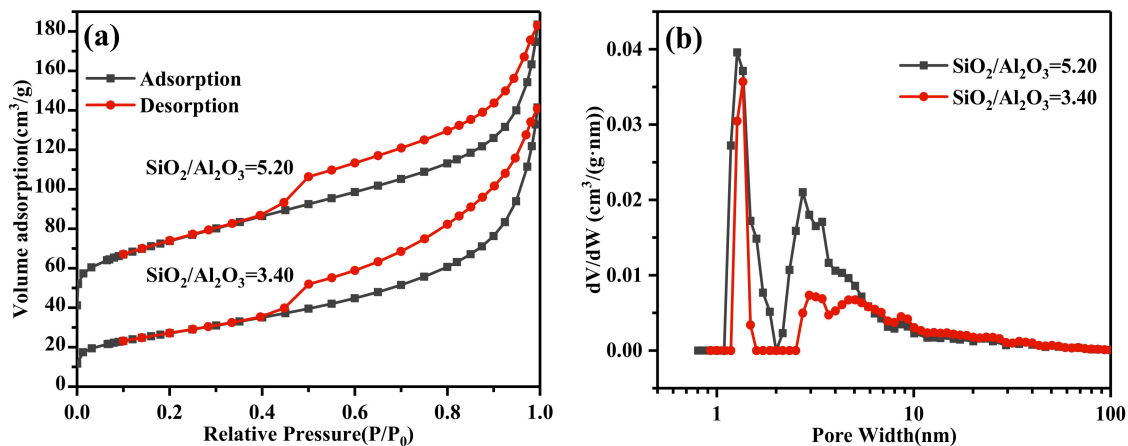
Figure 6. N_2 adsorption-desorption isotherms (**a**) and DFT pore size distribution curve (**b**) of zeolite NaP.

By comparing the results of SEM, FT-IR, TG-DSC, and BET, we found that, without adding a silicon aluminum source ($SiO_2/Al_2O_3 = 5.20$), the crystal morphology is more regular, the thermal stability is better, and the specific surface area is larger.

3.7. The NaP Zeolite to Remove Ammonia Nitrogen

The adsorption of ammonia nitrogen by NaP zeolite mainly depends on the ion exchange performance. The isomorphic substitution of Si and Al in the mineral structure will cause a negative charge in the zeolite channel and will be compensated by the exchange of sodium, calcium, magnesium and other ions. Secondly, the high-concentration ammonia-nitrogen solution can provide more exchange materials and form a larger concentration difference with the zeolite surface, thereby promoting the exchange of cations in NaP zeolite with NH_4^+ in the solution. Ion exchange is the main mechanism for NH_4^+ adsorption and is characterized by cation exchange capacity (CEC) [42–45].

3.7.1. Influence of Adsorbent Dosage

The relationship between the amount of NaP zeolite and the ammonia nitrogen removal rate and adsorption amount is shown in Figure 7. When the amount of zeolite was increased from 0.5 g/L to 40 g/L, the ammonia nitrogen removal rate increased from 13.55% to 93.83%, and the adsorption amount decreased from 21.11 mg/g to 2.35 mg/g. It can be seen that in the wastewater with an ammonia nitrogen concentration of 100 mg/L, increasing the amount of zeolite can significantly increase the removal rate of ammonia nitrogen. However, when the dosage of the adsorbent is more than 20 g/L, the ammonia nitrogen available for ion exchange decreases due to the decrease in the ammonia nitrogen concentration, and the agglomeration of the adsorbent increases, resulting in a slow increase in the ammonia nitrogen removal rate. Therefore, in the subsequent experiments, 20 g/L was selected as the optimal dosage of adsorbent [46–48].
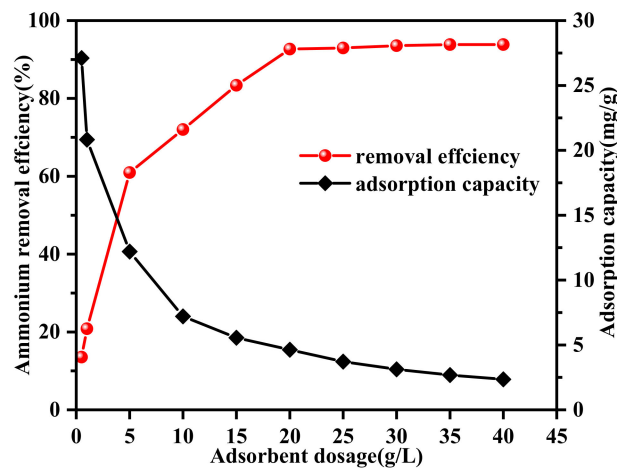
Figure 7. Effect of adsorbent dosage on Removal of ammonia nitrogen (pH = 7; contact time: 180 min).

3.7.2. Influence of pH

The adsorption of NaP zeolite on ammonia nitrogen in simulated wastewater with different pH values is shown in Figure 8. The ammonia nitrogen removal rate is proportional to the pH from 3 to 7, and inversely proportional to the pH from 7 to 10. Because under acidic conditions, the ammonia nitrogen in the wastewater mainly exists in the form of NH_4^+, a large amount of H^+ in the wastewater competes with NH_4^+ for adsorption, resulting in a decrease in the adsorption amount of ammonia nitrogen by the NaP zeolite. Under alkaline conditions, ammonia nitrogen in the wastewater exists in the form of molecular NH_3, resulting in a decrease in adsorption capacity. Therefore, the optimum removal rate of ammonia nitrogen by synthetic NaP zeolite is pH = 7. This is consistent with the better selectivity of the modified zeolite reported in the literature at pH = 7 [49,50].
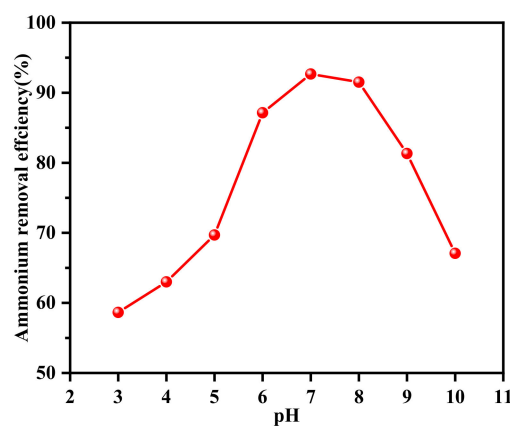

Figure 8. Effect of pH on ammonia nitrogen removal rate (adsorbent dosage: 20 g/L; contact time: 180 min).

3.7.3. Influence of Reaction Time

According to the curve of adsorption time and removal rate in Figure 9, it can be seen that NaP zeolite is fast for adsorption of ammonia nitrogen. When the time exceeds 180 min, the adsorption reaches equilibrium and the removal rate reaches over 92.67%. At this point, zeolite adsorption NH_4^+ reaches saturation, there will be ion exchange and adsorption equilibrium in the solution, even if the contact time is extended, the removal rate cannot be significantly increased [51]. Therefore, 180 min was selected as the optimal adsorption time.
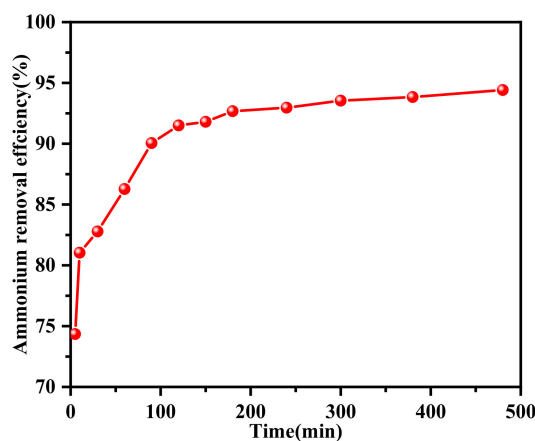
Figure 9. Effect of contact time on ammonia nitrogen removal rate (adsorbent dosage: 20 g/L; pH = 7).

Through the analysis of the above results, we can conclude that the dosage of NaP zeolite is directly proportional to the removal rate, and has the characteristics of fast adsorption and slow equilibrium. The pH value of the solution has a great effect on the removal of ammonia nitrogen by zeolite, and the removal effect is best under neutral conditions. The best adsorption parameters were: zeolite dosage of 20 g/L, solution pH = 7, and adsorption time of 180 min.

4. Conclusions

NaP zeolite with good physical properties can be synthesized by adding a small amount of NaOH and deionized water to the discarded CGCS. Adjust the molar ratio to $SiO_2:Al_2O_3:Na_2O:H_2O = 5.2:1.0:5.0:100$. This process does not require additional silicon source aluminum source and template agent, and does not require high temperature calcination. After aging for 24 h and crystallization at 105 °C for 12 h, NaP zeolite with high crystallinity and regular morphology and a specific surface area of 161.06 m^2/g can be obtained. The process has the characteristics of simple operation, low energy consumption, low cost, small secondary pollution, and easy industrialization. It is a resource utilization method of CGCS, and the water used in the process can be treated and recycled, which can basically achieve "zero discharge". The synthetic NaP zeolite has a good removal effect on ammonia nitrogen in industrial wastewater, the best removal rate is 92.67%, and the adsorption amount is 4.63 mg/g. Although the adsorption amount is not large, it has a large application prospect because of its simple preparation and low cost. Na^+ plays an important role in the formation of NaP zeolite crystals, and at the same time it can ion-exchange with NH_4^+, which is beneficial to the removal of ammonia nitrogen in wastewater.

Our work proposes a new way to solve the problems of large-scale accumulation, difficulty of utilization, huge environmental pressure, and high transportation cost of CGCS. The environmental functional materials prepared by CGCS can be applied to wastewater treatment in the industrial production process, which reduces the cost of the enterprise, realizes the resource utilization of waste, and achieves the purpose of "treating waste by waste".

References

1. Andrews, R.; Rubel, A.; Groppo, J.; Marrs, B. *Advanced Gasification by-Product Utilization*; Final Technical Report; University of Kentucky Center for Applied Energy Research: Lexington, KY, USA, 2006.

2. Zhao, X.; Zeng, C.; Mao, Y.; Li, W.; Peng, Y. The surface characteristics and reactivity of residual carbon in coal gasification slag. *Energy Fuels* **2009**, *24*, 91–94. [CrossRef]

3. Tang, Y.; Guo, X.; Xie, Q.; Finkelman, R.B.; Han, S. Petrological characteristics and trace element partitioning of gasification residues from slagging entrained-flow gasifiers in Ningdong, China. *Energy Fuels* **2018**, *32*, 3052–3067. [CrossRef]

4. Ge, J.C.; Yoon, S.K.; Choi, N.J. Application of fly ash as an adsorbent for removal of air and water pollutants. *Appl. Sci.* **2018**, *8*, 1116. [CrossRef]

5. Wu, S.; Huang, S.; Ji, L.; Wu, Y. Structure characteristics and gasification activity of residual carbon from entrained-flow coal gasification slag. *Fuel* **2014**, *122*, 67–75. [CrossRef]

6. Jun, Y.; Yoon, S.; Oh, J.E. A comparison study for chloride-binding capacity between alkali-activated fly ash and slag in the use of seawater. *Appl. Sci.* **2017**, *7*, 971. [CrossRef]

7. Yao, Z.T.; Ji, X.S.; Sarker, P.K.; Tang, J.H. A comprehensive review on the applications of coal fly ash. *Earth Sci. Rev.* **2015**, *141*, 105–121. [CrossRef]

8. Asl, S.M.H.; Ghadi, A.; Baei, M.S.; Javadian, H. Porous catalysts fabricated from coal fly ash as cost-effective alternatives for industrial applications: A review. *Fuel* **2018**, *217*, 320–342.

9. Liu, S.; Qi, C.; Jiang, Z.; Zhang, Y.; Niu, M.; Li, Y. Mineralogy and geochemistry of ash and slag from coal gasification in China: A review. *Int. Geol. Rev.* **2018**, *60*, 717–735. [CrossRef]

10. Li, C.C.; Qiao, X.C.; Yu, J.G. Large surface area MCM-41 prepared from acid leaching residue of coal gasification slag. *Mater. Lett.* **2016**, *167*, 246–249. [CrossRef]

11. Xu, Y.; Chai, X. Characterization of coal gasification slag-based activated carbon and its potential application in lead removal. *Environ. Technol.* **2018**, *39*, 382–391. [CrossRef]

12. Gu, Y.Y.; Qiao, X.C. A carbon silica composite prepared from water slurry coal gasification slag. *Microporous Mesoporous Mater.* **2019**, *276*, 303–307. [CrossRef]

13. Liu, S.; Chen, X.; Ai, W.; Wei, C. A new method to prepare mesoporous silica from coal gasification fine slag and its application in methylene blue adsorption. *J. Cleaner Prod.* **2019**, *212*, 1062–1071. [CrossRef]

14. Ji, Q.; Tabassum, S.; Hena, S.; Silva, C.G. A review on the coal gasification wastewater treatment technologies: Past, present and future outlook. *J. Cleaner Prod.* **2016**, *126*, 38–55. [CrossRef]

15. Tang, Y.; Wang, Y.; Huan, B.; Guo, X. Leachability of hazardous trace elements from entrained-flow coal gasification residues in Ningdong, China. *Energy Fuels* **2017**, *31*, 9703–9716. [CrossRef]

16. Tang, Y.; Guo, X.; Pan, X.; Finkelman, R.; Wang, Y. Changes and Distribution of Modes of Occurrence of Seventeen Potentially-Hazardous Trace Elements during Entrained Flow Gasification of Coals from Ningdong, China. *Minerals* **2018**, *8*, 202. [CrossRef]

17. Ministry of Ecology and Environment of People's Republic of China. *Water Quality-Determination of Ammonia Nitrogen-Nessler's Reagent Spectrophotometry*; Chinese standard HJ 535-2009; Ministry of Ecology and Environment of People's Republic of China: Pekin, China, 2010.

18. Ali, I.O.; Hassan, A.M.; Shaaban, S.M.; Soliman, K.S. Synthesis and characterization of ZSM-5 zeolite from rice husk ash and their adsorption of Pb^{2+} onto unmodified and surfactant-modified zeolite. *Sep. Purif. Technol.* **2011**, *83*, 38–44.

19. Kim, S.D.; Noh, S.H.; Park, J.W.; Kim, W.J. Organic-free synthesis of ZSM-5 with narrow crystal size distribution using two-step temperature process. *Microporous Mesoporous Mater.* **2006**, *92*, 181–188. [CrossRef]

20. Kim, S.D.; Noh, S.H.; Seong, K.H.; Kim, W.J. Compositional and kinetic study on the rapid crystallization of ZSM-5 in the absence of organic template under stirring. *Microporous Mesoporous Mater.* **2004**, *72*, 185–192. [CrossRef]

21. Ali, I.O.; El-Sheikh, S.M.; Salama, T.M.; Bakr, M.F. Controllable synthesis of NaP zeolite and its application in calcium adsorption. *Sci. China Mater.* **2015**, *58*, 621–633. [CrossRef]

22. Liu, Y.; Yan, C.; Zhang, Z.; Wang, H.; Zhou, S.; Zhou, W. A comparative study on fly ash, geopolymer and faujasite block for Pb removal from aqueous solution. *Fuel* **2016**, *185*, 181–189. [CrossRef]

23. Zhang, Z.; Wang, H.; Provis, J.L. Quantitative study of the reactivity of fly ash in geopolymerization by FTIR. *J. Sustain. Cem. Based Mater.* **2012**, *1*, 154–166. [CrossRef]

24. Cardoso, A.M.; Paprocki, A.; Ferret, L.S.; Azevedo, C.M. Synthesis of zeolite Na-P1 under mild conditions using Brazilian coal fly ash and its application in wastewater treatment. *Fuel* **2015**, *139*, 59–67. [CrossRef]

25. Cardoso, A.M.; Horn, M.B.; Ferret, L.S.; Azevedo, C.M. Integrated synthesis of zeolites 4A and Na–P1 using coal fly ash for application in the formulation of detergents and swine wastewater treatment. *J. Hazard. Mater.* **2015**, *287*, 69–77. [CrossRef] [PubMed]

26. Sánchez-Hernández, R.; López-Delgado, A.; Padilla, I.; Galindo, R. One-step synthesis of NaP1, SOD and ANA from a hazardous aluminum solid waste. *Microporous Mesoporous Mater.* **2016**, *226*, 267–277. [CrossRef]

27. Albert, B.R.; Cheetham, A.K.; Stuart, J.A.; Adams, C.J. Investigations on P zeolites: Synthesis, characterisation, and structure of highly crystalline low-silica NaP. *Microporous Mesoporous Mater.* **1998**, *21*, 133–142. [CrossRef]

28. Liu, Y.; Yan, C.; Qiu, X.; Li, D.; Wang, H. Preparation of faujasite block from fly ash-based geopolymer via in-situ hydrothermal method. *J. Taiwan Inst. Chem. Eng.* **2016**, *59*, 433–439. [CrossRef]

29. Rayalu, S.S.; Udhoji, J.S.; Meshram, S.U.; Naidu, R.R. Estimation of crystallinity in fly ash-based zeolite-A using XRD and IR spectroscopy. *Curr. Sci.* **2005**, *89*, 2147–2151.

30. Yao, Y.; Sun, H. A novel silica alumina-based backfill material composed of coal refuse and fly ash. *J. Hazard. Mater.* **2012**, *213*, 71–82. [CrossRef]

31. Stevens, R.W., Jr.; Siriwardane, R.V.; Logan, J. In situ Fourier transform infrared (FT-IR) investigation of CO_2 adsorption onto zeolite materials. *Energy Fuels* **2008**, *22*, 3070–3079. [CrossRef]

32. Sharma, P.; Song, J.S.; Han, M.H.; Cho, C.H. GIS-NaP1 zeolite microspheres as potential water adsorption material: Influence of initial silica concentration on adsorptive and physical/topological properties. *Sci. Rep.* **2016**, *6*, 22734. [CrossRef]

33. Bohra, S.; Kundu, D.; Naskar, M.K. Synthesis of cashew nut-like zeolite NaP powders using agro-waste material as silica source. *Mater. Lett.* **2013**, *106*, 182–185. [CrossRef]

34. Huo, Z.; Xu, X.; Lü, Z.; Song, J.; He, M. Synthesis of zeolite NaP with controllable morphologies. *Microporous Mesoporous Mater.* **2012**, *158*, 137–140. [CrossRef]

35. Liu, Y.; Yan, C.; Zhao, J.; Zhang, Z.; Wang, H. Synthesis of zeolite P1 from fly ash under solvent-free conditions for ammonium removal from water. *J. Cleaner Prod.* **2018**, *202*, 11–22. [CrossRef]

36. Koshy, N.; Jha, B.; Kadali, S.; Singh, D.N. Synthesis and characterization of Ca and Na zeolites (non-pozzolanic materials) obtained from fly Ash-Ca $(OH)_2$ interaction. *Mater. Perform. Charact.* **2015**, *4*, 87–102.

37. Sing, K.S. Reporting physisorption data for gas/solid systems with special reference to the determination of surface area and porosity (Recommendations 1984). *Pure Appl. Chem.* **1985**, *57*, 603–619. [CrossRef]

38. Bandura, L.; Franus, M.; Józefaciuk, G.; Franus, W. Synthetic zeolites from fly ash as effective mineral sorbents for land-based petroleum spills cleanup. *Fuel* **2015**, *147*, 100–107. [CrossRef]

39. Zhou, C.; Gao, Q.; Luo, W.; Zhou, Q.; Wang, H. Preparation, characterization and adsorption evaluation of spherical mesoporous Al-MCM-41 from coal fly ash. *J. Taiwan Inst. Chem. Eng.* **2015**, *52*, 147–157. [CrossRef]

40. Aldahri, T.; Behin, J.; Kazemian, H.; Rohani, S. Synthesis of zeolite Na-P from coal fly ash by thermo-sonochemical treatment. *Fuel* **2016**, *182*, 494–501. [CrossRef]

41. Majchrzak-Kucęba, I.; Nowak, W. A thermogravimetric study of the adsorption of CO_2 on zeolites synthesized from fly ash. *Thermochim. Acta* **2005**, *437*, 67–74. [CrossRef]

42. Nasir, N.; Daud, Z.; Abd Kadir, A.; Latiff, A.A.A.; Ahmad, B.; Suhani, N.; Halim, A.A. Removal of ammonia nitrogen from rubber industry wastewater using zeolite as adsorbent. *Malays. J. Fundam. Appl. Sci.* **2019**, *15*, 862–866.

43. Huo, H.; Lin, H.; Dong, Y.; Cheng, H.; Wang, H.; Cao, L. Ammonia-nitrogen and phosphates sorption from simulated reclaimed waters by modified clinoptilolite. *J. Hazard. Mater.* **2012**, *229*, 292–297. [CrossRef] [PubMed]

44. Wang, H.; Gui, H.; Yang, W.; Li, D.; Tan, W.; Yang, M.; Barrow, C.J. Ammonia nitrogen removal from aqueous solution using functionalized zeolite columns. *Desalin. Water Treat.* **2014**, *52*, 753–758. [CrossRef]

45. Kizito, S.; Wu, S.; Kirui, W.K.; Lei, M.; Lu, Q.; Bah, H.; Dong, R. Evaluation of slow pyrolyzed wood and rice husks biochar for adsorption of ammonium nitrogen from piggery manure anaerobic digestate slurry. *Sci. Total Environ.* **2015**, *505*, 102–112. [CrossRef] [PubMed]

46. Zhang, M.; Zhang, H.; Xu, D.; Han, L.; Niu, D. Removal of ammonium from aqueous solutions using zeolite synthesized from fly ash by a fusion method. *Desalination* **2011**, *271*, 111–121. [CrossRef]

47. Arslan, A.; Veli, S. Zeolite 13X for adsorption of ammonium ions from aqueous solutions and hen slaughterhouse wastewaters. *J. Taiwan Inst. Chem. Eng.* **2012**, *43*, 393–398. [CrossRef]

48. Behin, J.; Bukhari, S.S.; Kazemian, H.; Rohani, S. Developing a zero liquid discharge process for zeolitization of coal fly ash to synthetic NaP zeolite. *Fuel* **2016**, *171*, 195–202. [CrossRef]

49. He, Y.; Lin, H.; Dong, Y.; Liu, Q.; Wang, L. Simultaneous removal of ammonium and phosphate by alkaline-activated and lanthanum-impregnated zeolite. *Chemosphere* **2016**, *164*, 387–395. [CrossRef]

50. Thornton, A.; Pearce, P.; Parsons, S.A. Ammonium removal from solution using ion exchange on to MesoLite, an equilibrium study. *J. Hazard. Mater.* **2007**, *147*, 883–889. [CrossRef]

51. Saltalı, K.; Sarı, A.; Aydın, M. Removal of ammonium ion from aqueous solution by natural Turkish (Yıldızeli) zeolite for environmental quality. *J. Hazard. Mater.* **2007**, *141*, 258–263. [CrossRef]